

● *Original Contribution*

IDENTIFYING THE INERTIAL CAVITATION THRESHOLD AND SKULL EFFECTS IN A VESSEL PHANTOM USING FOCUSED ULTRASOUND AND MICROBUBBLES

YAO-SHENG TUNG,* JAMES J. CHOI,* BABAK BASERI,* and ELISA E. KONOFAGOU*†

*Department of Biomedical Engineering, Columbia University, New York, New York, USA; and †Department of Radiology, Columbia University, New York, New York, USA

(Received 24 April 2009; revised 17 February 2010; in final form 22 February 2010)

Abstract—Focused ultrasound (FUS) in combination with microbubbles has been shown capable of delivering large molecules to the brain parenchyma through opening of the blood-brain barrier (BBB). However, the mechanism behind the opening remains unknown. To investigate the pressure threshold for inertial cavitation of preformed microbubbles during sonication, passive cavitation detection in conjunction with B-mode imaging was used. A cerebral vessel was simulated by generating a cylindrical hole of 610 μm in diameter inside a polyacrylamide gel and saturating its volume with microbubbles. Definity microbubbles (Mean diameter range: 1.1–3.3 μm , Lantheus Medical Imaging, N. Billerica, MA, USA) were injected prior to sonication (frequency: 1.525 MHz; pulse length: 100 cycles; PRF: 10 Hz; sonication duration: 2 s) through an excised mouse skull. The acoustic emissions due to the cavitation response were passively detected using a cylindrically focused hydrophone, confocal with the FUS transducer and a linear-array transducer with the field of view perpendicular to the FUS beam. The broadband spectral response acquired at the passive cavitation detector (PCD) and the B-mode images identified the occurrence and location of the inertial cavitation, respectively. Findings indicated that the peak-rarefactional pressure threshold was approximately equal to 0.45 MPa, with or without the skull present. Mouse skulls did not affect the threshold of inertial cavitation but resulted in a lower inertial cavitation dose. The broadband response could be captured through the murine skull, so the same PCD set-up can be used in future *in vivo* applications. (E-mail: ek2191@columbia.edu) © 2010 World Federation for Ultrasound in Medicine & Biology.

Key Words: Blood-brain barrier, BBB, Cavitation, Microbubble, Skull, Inertial, Vessel, Pressure.

INTRODUCTION

It has been demonstrated that focused ultrasound (FUS) combined with microbubbles can open the blood-brain barrier (BBB) *in vivo* at acoustic pressures and duty cycles low enough that significant thermal effects may be avoided (Hynynen et al. 2001; Choi et al. 2007b). Neuronal damage throughout the sonicated region, as analyzed in histology, was not observed at acoustic pressures close to the threshold of BBB opening (McDannold et al. 2005). Different ultrasound contrast agents (UCA) and acoustic parameters such as frequency, pulse repetition frequency (PRF) and burst length have also been investigated. The pressure threshold of BBB opening was shown to decrease with burst length while the PRF did not affect the threshold (McDannold et al.

2008b). The mechanical index (MI) may also be an important indicator for predicting BBB opening (McDannold et al. 2008a). The acoustic pressure threshold for BBB opening was shown to increase with the applied sonication frequency. However, the threshold remained constant compared with the mechanical index.

The mechanism of BBB opening remains largely uncovered. Not only is the interaction between the acoustically driven bubble and brain capillaries unknown but also the effect of the skull on the BBB opening threshold has not been thoroughly described. Several studies investigating BBB opening require craniotomy (Hynynen et al. 2001; McDannold et al. 2005, 2006, 2007, 2008b). However, craniotomy is a difficult and time-consuming process that is associated with brain exposure, morbidity and occasional mortality. As a result, a lower frequency (260 kHz) has been proposed, which resulted in lower aberration through the skull when opening the BBB transcranially (Hynynen et al. 2005, 2006). Our group has characterized the FUS beam through the mouse skull in

Address correspondence to: Dr. Elisa E. Konofagou, Department of Biomedical Engineering, Columbia University, 351 Engineering Terrace, mail code 8904 1210 Amsterdam Avenue, New York, NY 10027 USA. E-mail: ek2191@columbia.edu

simulations and *ex vivo* skull experiments to study the effects of aberration and attenuation through the skull (Choi *et al.* 2007a). Localized, transcranial BBB opening in the murine hippocampus has also been reported (Choi *et al.* 2007b; Choi *et al.* 2010a; 2010b).

Acoustic cavitation, which refers to acoustically driven bubble activity, is considered to be the main cause for inducing BBB opening since it does not occur without injecting preformed microbubbles at a given acoustic setting. At low acoustic pressures, acoustically driven UCA size oscillations were shown to increase the permeability of surrounding cell membranes (van Wamel *et al.* 2004). At high acoustic pressures, inertial cavitation, *i.e.*, the collapse of bubbles, releases high energy and may create high temperatures, high pressures, and high velocity jets that may damage the surrounding structures (Miller *et al.* 1996). Therefore, knowing the pressure threshold for inducing inertial cavitation is important for controlling the effects induced by acoustically driven microbubbles. Apfel and Holland calculated the pressure threshold of inertial cavitation in water and showed that it increased with frequency (Apfel and Holland 1991). Most studies on the threshold of cavitation effects with UCA were based on the assumption of a free microbubble *i.e.*, not contained in a vessel phantom (Chomas *et al.* 2001a, 2001b; Giesecke and Hynynen 2003; Chen *et al.* 2003a, 2003b; Ammi *et al.* 2006). However, containment of the bubble within a vessel alters its behavior. Using theoretical and experimental evaluation in gel phantoms, Sassaroli and Hynynen reported that the threshold of inertial cavitation would be higher as the vessel diameter decreased as long as the diameter remained under 300 microns (Sassaroli and Hynynen 2006, 2007). Qin and Ferrara simulated the interaction between acoustically driven microbubbles in compliant and rigid microvessels and found that the threshold of bubble fragmentation was higher within rigid vessels when compared with compliant vessels (Qin and Ferrara 2006).

The relationship between acoustic cavitation and BBB disruption was previously investigated using a ring-shaped passive cavitation detector (PCD) surrounding a sonication transducer (McDannold *et al.* 2005, 2006). The peak-rarefactional pressure threshold of BBB opening and inertial cavitation at 260 kHz was found to be 0.29 MPa and 0.40 MPa, respectively, which suggested that inertial cavitation might not be necessary for BBB opening. However, the studies were performed following craniotomy and ignored any effects that the skull may introduce such as a change in the threshold of inertial cavitation.

The purpose of this paper was to investigate the effects of the mouse skull on the peak-rarefactional pressure threshold of inertial cavitation in a vessel phantom. *Ex vivo* mouse skulls were placed on the phantom to study transcranial wave propagation. The occurrence of inertial

cavitation was investigated using simultaneous PCD and B-mode imaging. We also determined whether the cavitation response changes when the same acoustic pressures were applied at the presence or absence of the murine skull. At each pressure, different function generator voltages were applied to obtain the same acoustic pressure both in the presence and absence of the skull. The inertial cavitation dose (ICD) was used to identify the threshold of inertial cavitation and quantify the broadband response.

MATERIALS AND METHODS

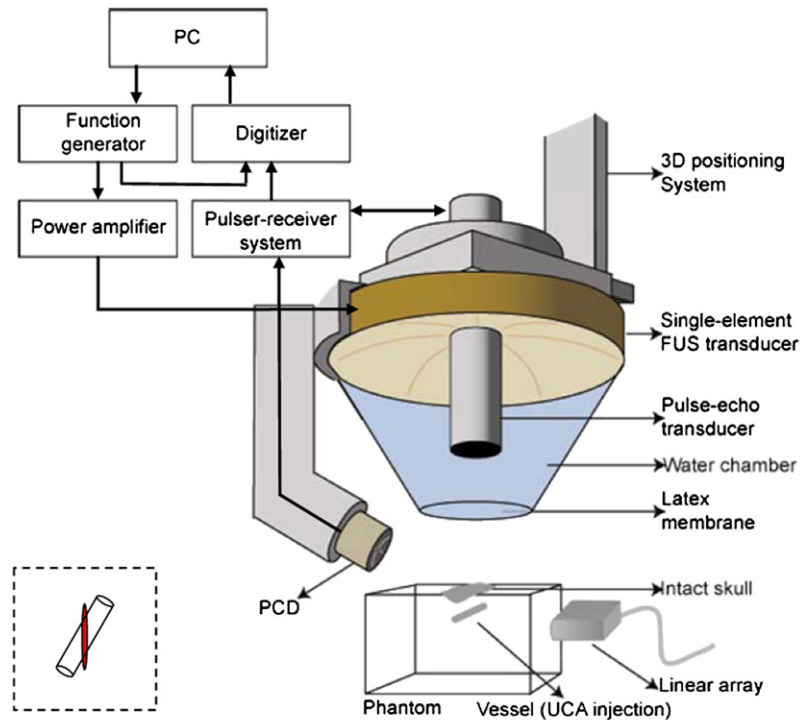
Experimental set-up

The experimental set-up is shown in Figure 1. A single-element circular focused ultrasound transducer (Riverside Research Institute, New York, NY, USA) was driven by a function generator (Agilent Technologies, Palo Alto, CA, USA) through a 50-dB power amplifier (ENI Inc., Rochester, NY, USA). The center frequency, focal depth, outer radius and inner radius of the FUS transducer were 1.525 MHz, 90 mm, 30 mm and 11.2 mm, respectively. A single-element diagnostic transducer (center frequency: 7.5 MHz, focal length: 60 mm), which was driven by a pulser-receiver (Panametrics, Waltham, MA, USA), was positioned through the opening of the FUS transducer. These two transducers were confocally aligned. A cone filled with degassed and distilled water was attached to the transducer assembly. The transducer was then mounted on a computer-controlled positioner (Velmex Inc., Bloomfield, NY, USA). The dimensions of the focal region were measured and a lateral and axial full-width at half maximum (FWHM) intensity were of approximately 1.32 and 13.0 mm, respectively.

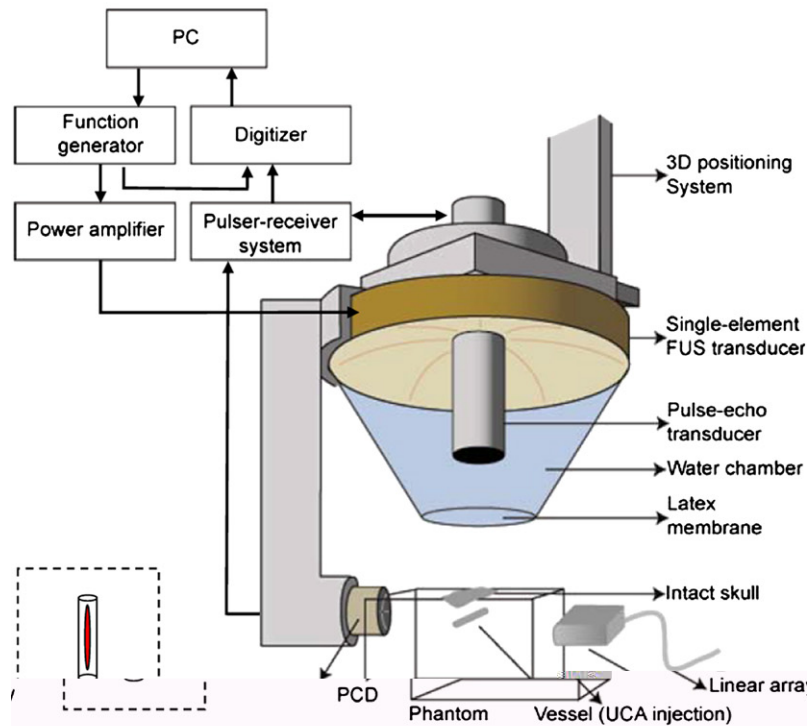
A 5-cm broadband, cylindrically focused hydrophone (Sonic Concepts, Bothell, WA, USA) with a cylindrical focal region (height 19 mm, diameter 3.64 mm) was placed at 60° (60°-PCD, Fig. 1a) or 90° (90°-PCD, Fig. 1b) from the longitudinal axis of the FUS beam. The hydrophone holder was adjusted to confocally align the hydrophone and the FUS transducer. The acoustic emissions from the microbubbles were acquired by the hydrophone followed by a 20-dB amplification (model 5800; Olympus NDT, Waltham, MA, USA) and collected using a digitizer (model 14200; Gage Applied Technologies, Inc., Lachine, QC, Canada).

Each sonication set included a pulse length of 100 cycles (67 μ s) and a pulse repetition frequency (PRF) of 10 Hz. The total sonication duration of a sonication set was 2 s, *i.e.*, 20 pulses. Acoustic signals emitted from microbubbles were acquired for each pulse. The peak-rarefactional pressure amplitude ranged between 0.30 and 0.90 MPa at a 0.15 MPa step size as calibrated in our previous studies (Choi *et al.* 2007b).

The vessel phantom was constructed using acrylamide following Takegami *et al.* without the egg protein



a



b

Fig. 1. Block diagram of the experimental set-up. The passive cavitation detector (PCD) was positioned at a (a) 60° and (b) 90° from the longitudinal axis of the focused ultrasound (FUS) beam. The space between the latex membrane and the phantom indicated degassed water. The overlap between the focal region of PCD and FUS was illustrated in the insets. The cylindrical region was the focal region of PCD and the cigar-shaped region was the focal region of FUS. The water tank, in which the phantom was immersed, is not shown for clarity purposes.

(Takegami *et al.* 2004). The vessel was formed by inserting a polyethylene tube (model PE10; Becton Dickinson and Company, Sparks, MD, USA) before the phantom solidified and removing it immediately after. The phantom was immersed in a tank filled with degassed water (Fig. 1). The vessel was positioned 3 mm below the surface of the phantom to simulate the location of the vessel targeted in the *in vivo* application (Choi *et al.* 2007a, 2007b). A linear-array transducer (center frequency 7.5 MHz, model 10L5; Terason Ultrasound, Burlington, MA, USA) was placed perpendicular to the longitudinal axis of the FUS transducer (Fig. 1) and was used to map the spatial distribution of microbubbles after sonication.

Skull preparation and targeting procedure

Three brown mice (strain: C57BL/6, sex: male, mass: 20–25 g) were euthanized, their skulls were extracted and then immersed into a formalin solution. All procedures used on the mice were approved by the Columbia University Institutional Animal Care and Use Committee. The thickness of the parietal bone was 0.18, 0.20 and 0.23 mm, respectively. The intact skull was degassed before each experiment to prevent any cavitation effects at the skull level that may affect the beam propagation. Based on previous experiments, the skull attenuates the pressure amplitude by approximately 18.1% at 1.525 MHz (Choi *et al.* 2007b). Therefore, the FUS transducer was driven at different voltages to ensure that the pressure values were of the same magnitude, with or without the skull in place.

Figure 2 illustrates the targeting method through the skull that is also used *in vivo* to open the BBB in

a subcortical structure such as the hippocampus (Choi *et al.* 2007b). Since the thickness and attenuation of the skull vary across its volume, a precise targeting method was required to propagate through the thinnest region. A grid-positioning method was used to ensure that the focal spot overlapped with the equivalent hippocampus location, which is the target in our *in vivo* studies (Choi *et al.* 2007a, 2007b). First, a raster scan (Fig. 2a) was performed to ensure that the center of the FUS focal spot was placed in the middle of the vessel. Second, the FUS transducer was positioned above the skull. A second raster scan was performed to locate the region equivalent to the hippocampus location *in vivo*, *i.e.*, 3 mm below the skull as indicated in Fig. 2b.

Microbubble preparation and sonication

Definity microbubbles (Bristol-Myers Squibb Medical Imaging, N. Billerica, MA, USA), which constitute perflutren-filled, lipid-shelled microspheres, were used in our experiments. These microbubbles had a mean diameter of about 1.1 to 3.3 μm , with 98% having a diameter lower than 10 μm and a concentration of around 1.2×10^{10} bubbles/mL. In this study, the concentration was diluted in degassed phosphate buffered saline (PBS) to 2.5×10^7 (number of bubbles/mL), which approximated what has been used in previous *in vivo* studies (Choi *et al.* 2007a, 2007b). The concentration (number of bubbles/mL) of microbubbles was measured by a particle sizer (Accusizer 780A; NICOMP Particle Sizing Systems, Santa Barbara, CA, USA), which used a laser light obscuration and scattering technique. To ensure that

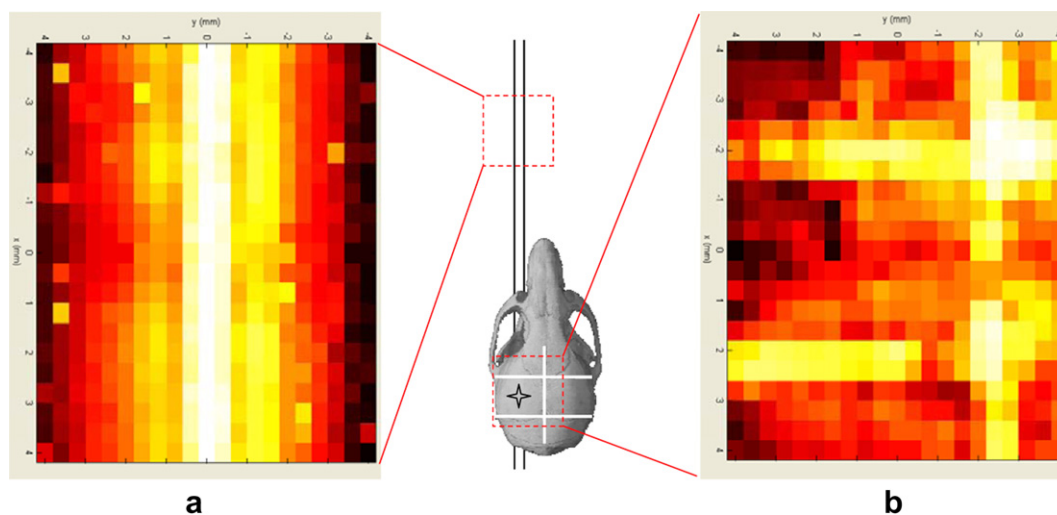


Fig. 2. The vessel below the *ex vivo* mouse skull was located using raster scan with the pulse-echo transducer. (a) The first raster scan was used to find the position of the vessel while (b) the second raster scan was used to find the position of the left parietal bone, where in previous studies was the acoustic window through which to sonicate to target the left-hippocampus region (star symbol). The white bar indicates the grid which was yellow shown in (b). The image of the mouse skull is publicly available at <http://www.digimorph.org>.

the concentration of the microbubbles did not change over time, *e.g.*, caused by a decay of microbubbles, a new batch of diluted bubble suspension was used every 10 min. The same diluted bubble suspension was used for 10 independent sonication sets.

At each pressure amplitude and PCD angle, five sonication sets were performed in the presence and five in the absence, of the skull. A new phantom was made when a new skull was used, each for 15 to 20 sonication sets. Prior to each sonication set, new microbubbles were slowly injected into the vessel formed to avoid any change in the microbubble size distribution and concentration that may be introduced with a fast bubble injection (Talu et al. 2008). Following each sonication set, degassed water was used to remove any remaining microbubbles inside the vessel.

Data acquisition and analysis

The acoustic emissions acquired by the PCD were sampled at 80 MHz and processed using MATLAB (2007b; Mathworks, Natick, MA, USA). The resulting signals were analyzed using four independent methods: the frequency response of the first pulse of each sonication was obtained using a 4096-point FFT (Fig. 3), a spectrogram depicting the frequency response of the signal versus the 20 sonication pulses applied (Fig. 4), the root mean square (RMS) of the PCD's recorded voltage amplitude (V_{RMS}) for each pulse (Fig. 5a) and the average across all pulses (Fig. 5b).

In the calculation of the V_{RMS} and ICD, a highpass filter with a cut-off of 4 MHz was first applied to the acquired PCD signal. A comb filter was then used to exclude the ± 150 kHz range at the transducer's harmonic (nf , $n = 1, 2, \dots, 6$), subharmonic ($f/2$) and ultraharmonic ($nf/2$, $n = 3, 5, 7, 9$) frequencies (Famy et al. 2009). The ICD was defined as the integral of the area under the V_{RMS} curve over the 2-s sonication duration. To reduce the noise in the ICD calculation, the V_{RMS} of water at each pressure amplitude was also calculated and was subtracted from the results of the bubble experiment to obtain the net bubble response.

Radiofrequency (RF) data from the linear array was acquired using the Terason system and processed using MATLAB. B-mode imaging was then performed using the Hilbert function on the acquired RF data. The change in the B-mode imaging contrast due to microbubbles was calculated as the intensity ratio:

$$\text{Intensity ratio} = \frac{I_{pre} - I_{post}}{I_{pre}} \quad (1)$$

where I_{pre} is the intensity of the region-of-interest (ROI) at the FUS focal region before sonication and I_{post} is the intensity of the ROI after sonication. The dimension of the ROI was equal to 9.0×7.2 mm².

A Student's *t*-test was used to determine whether the ICD dose or intensity ratio was different between the two different pressures. A *p* value of $p < 0.05$ was considered to represent a significant difference in all comparisons.

In vivo cavitation detection

The FUS set-up was the same as the one in our phantom experiments and the 60°-PCD was used for *in vivo* cavitation detection during BBB opening. Fifty microliters (50 μ L) of original microbubble concentration per kilogram of mouse body weight was used for BBB opening. Sonication started 1 min after bubble injection (frequency: 1.525 MHz; peak-rarefactional pressure: 0.30, 0.45 and 0.60 MPa; pulse length: 30400 cycles (20 ms); PRF: 10 Hz; sonication duration: 60 s with a 30-s interval). Only the right hippocampus was sonicated while the left hippocampus was not targeted and was used as the control case. The acoustic signals acquired by the same broadband focused hydrophone were processed using a Matlab function (spectrogram; 492 samples Chebyshev window; 95% overlap; 4096-point FFT) to determine the onset of broadband response.

RESULTS

The frequency response of the first pulse as recorded by the 60°-PCD and 90°-PCD configurations, with and without the presence of the skull in the wave propagation path is depicted in Figure 3. Without the skull, the frequency spectra in the 60°-PCD and 90°-PCD cases are similar. The frequency response shown in this study can be classified into two categories (Leighton 1994). The first response is generated by stable cavitation, *i.e.*, at harmonic, subharmonic and ultraharmonic frequencies. The second response is generated by inertial cavitation, which will produce broadband acoustic emission. Here, the broadband response was detected when the pressure was at, or higher than, 0.45 MPa (Fig. 3a and c). This broadband response was used to determine the threshold of inertial cavitation for Definity within the 610-micron-diameter vessel. The skull presence led to a decrease in the peak amplitude of all harmonics, but the characteristic broadband response was still detected (Fig. 3b and d). This indicated that the threshold of inertial cavitation of 0.45 MPa was not dependent on the skull presence. However, comparison of the results between the 60°-PCD and 90°-PCD configurations showed that the detection of acoustic emissions was influenced by the skull's presence, *i.e.*, part of the broadband response was absorbed by the skull (Fig. 3b).

To understand the temporal behavior of the bubbles, the frequency response's temporal variation was studied using spectrograms at the two different PCD angles with and without the skull (Fig. 4). The spectrogram also indicated that the skull influences the signal at 60°-PCD. The

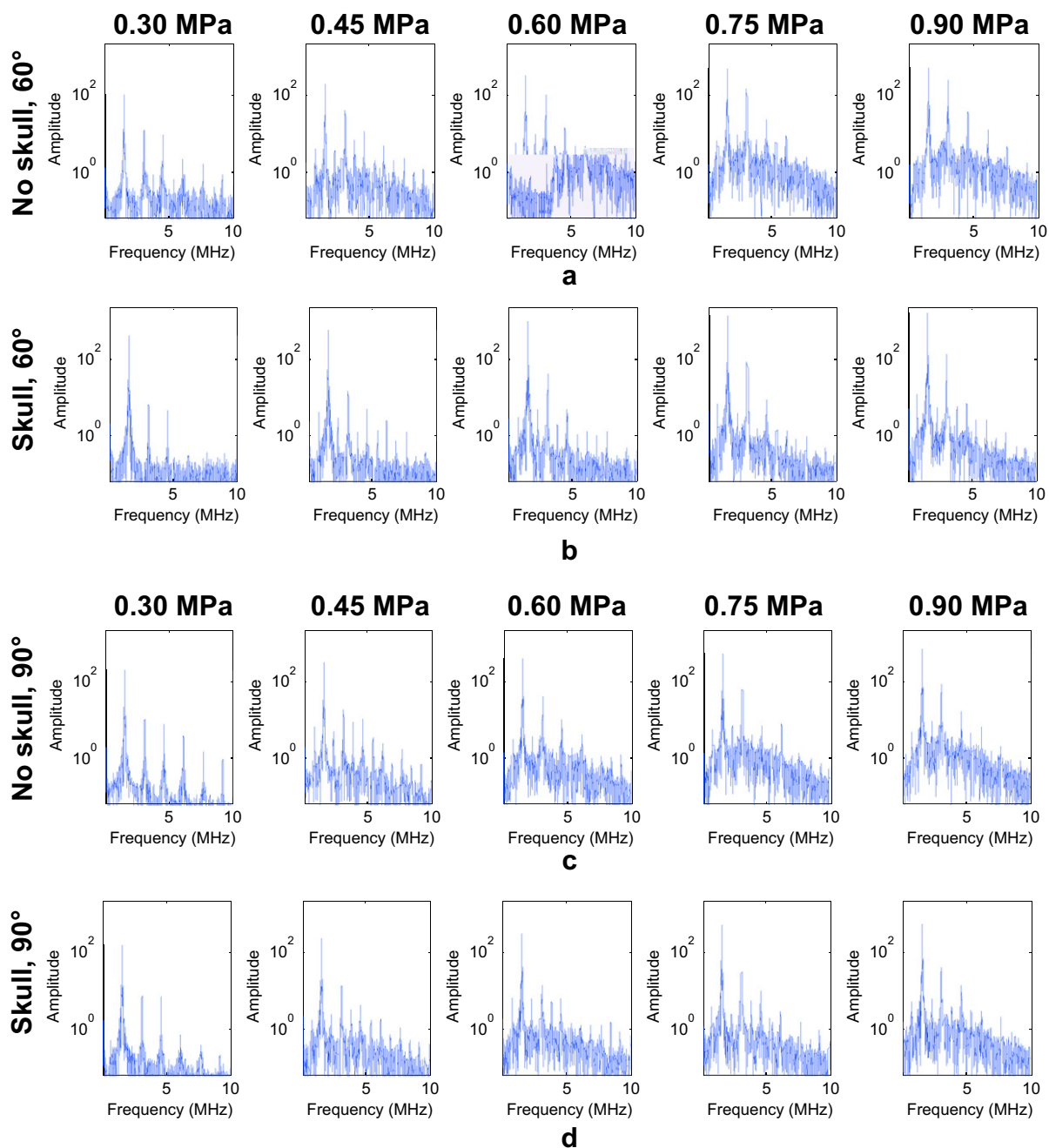


Fig. 3. Frequency response of the first pulse (a, c) through no skull and (b, d) through an *ex vivo* skull at five distinct acoustic pressures. Acoustic emissions were collected with a PCD positioned at (a, b) 60° and (c, d) 90° relative to the longitudinal axis of the focused ultrasound (FUS) beam. Broadband acoustic emissions were detected at and higher than 0.45 MPa.

amplitude around the fundamental frequency was enhanced by the skull (Fig. 4b). However, both Figures 3 and 4 confirm the threshold of inertial cavitation to be at 0.45 MPa.

The broadband response as detected by the PCD was quantified by using the V_{RMS} at each pressure amplitude (Fig. 5a) and the ICD (Fig. 5b). The ICD, which is shown in Figure 5b, was calculated by integrating V_{RMS} . The V_{RMS} curve depicted no significant difference between

different pressure amplitudes beyond 1 s. As indicated by the ICD calculations (Fig. 5b), the presence of the skull induced lower ICD and the ICD at 60° -PCD was lower than at 90° -PCD. The ICD at 0.45 MPa was statistically higher than at 0.30 MPa ($p < 0.05$), which confirmed that the threshold of inertial cavitation was around 0.45 MPa.

B-mode images acquired after 2 s of sonication were used to depict the spatial distribution of microbubbles within the vessel at five different pressure amplitudes,

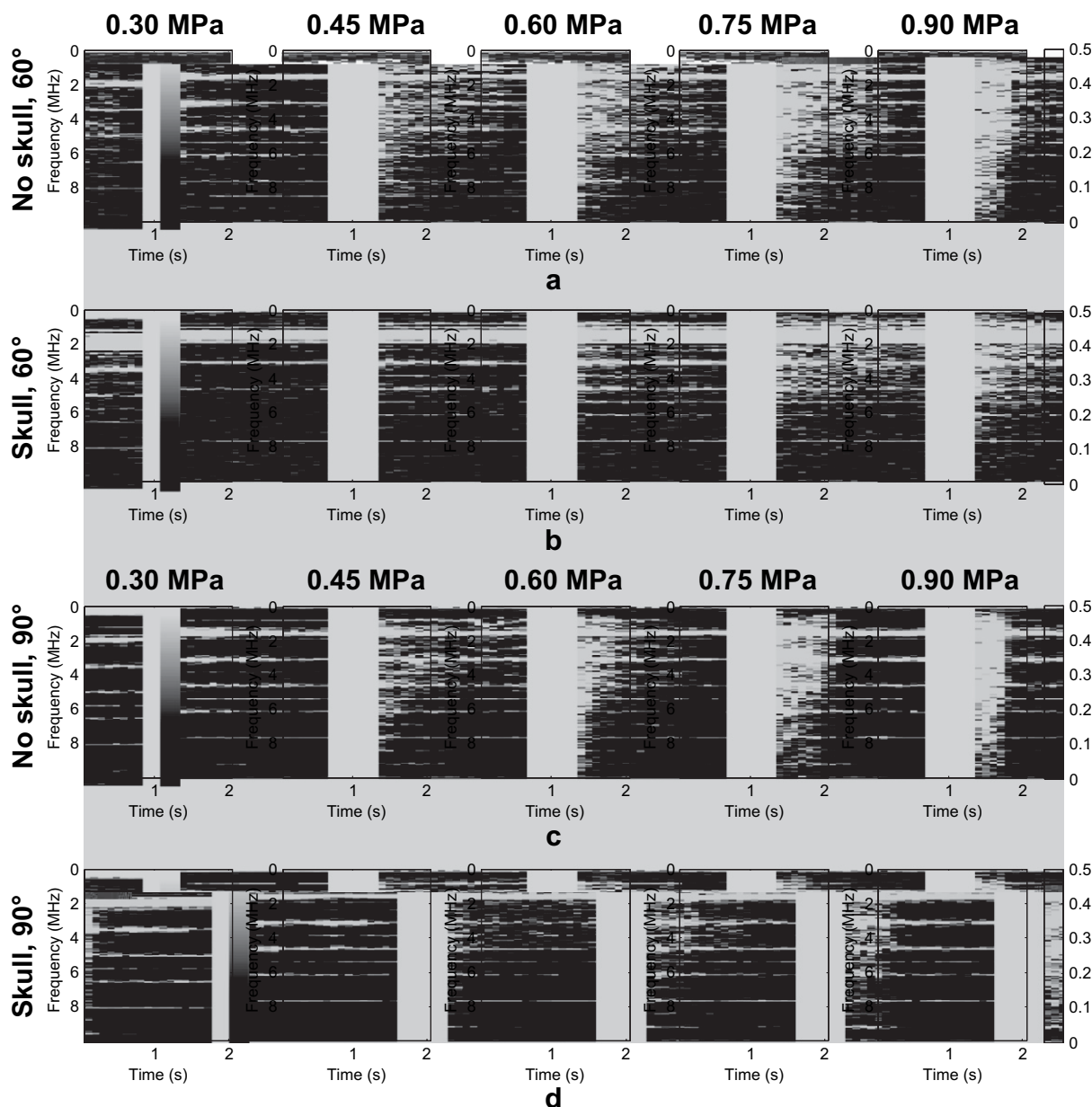


Fig. 4. The spectrogram (a, c) without the skull and (b, d) through an *ex vivo* skull at five distinct acoustic pressures. The duration of each sonication was 2 s, *i.e.*, 20 pulses. Please note that the broadband acoustic emissions could only be detected at the first two pulses at 0.45 MPa in (b) and their amplitudes were much lower than at higher pressures.

with or without skull (Fig. 6). As the pressure amplitude increased, an increasingly dark region in the center of the B-mode image coinciding with the FUS focus (Fig. 7a), representing loss of echogenicity, was observed in the focal region. With the skull in place, the dark region appeared only when the pressure amplitude was at or above 0.45 MPa, which was consistent with the aforementioned threshold of inertial cavitation from the PCD (Fig. 5). The spatial maps were compared against the ICD measurements. The region-of-interest (ROI) around the focal region of FUS was traced and the intensity ratio (eqn [1]) decrease

was calculated from the radio frequency (RF) data corresponding to the B-mode images (Fig. 7a). The intensity ratio was found to be statistically different between 0.30 MPa and 0.45 MPa ($p < 0.05$) (Fig. 7b). This was also consistent with the results of the ICD quantification.

DISCUSSION

The peak-rarefactional pressure threshold of inertial cavitation in the presence of preformed microbubbles in a vessel phantom by FUS in the absence or presence of

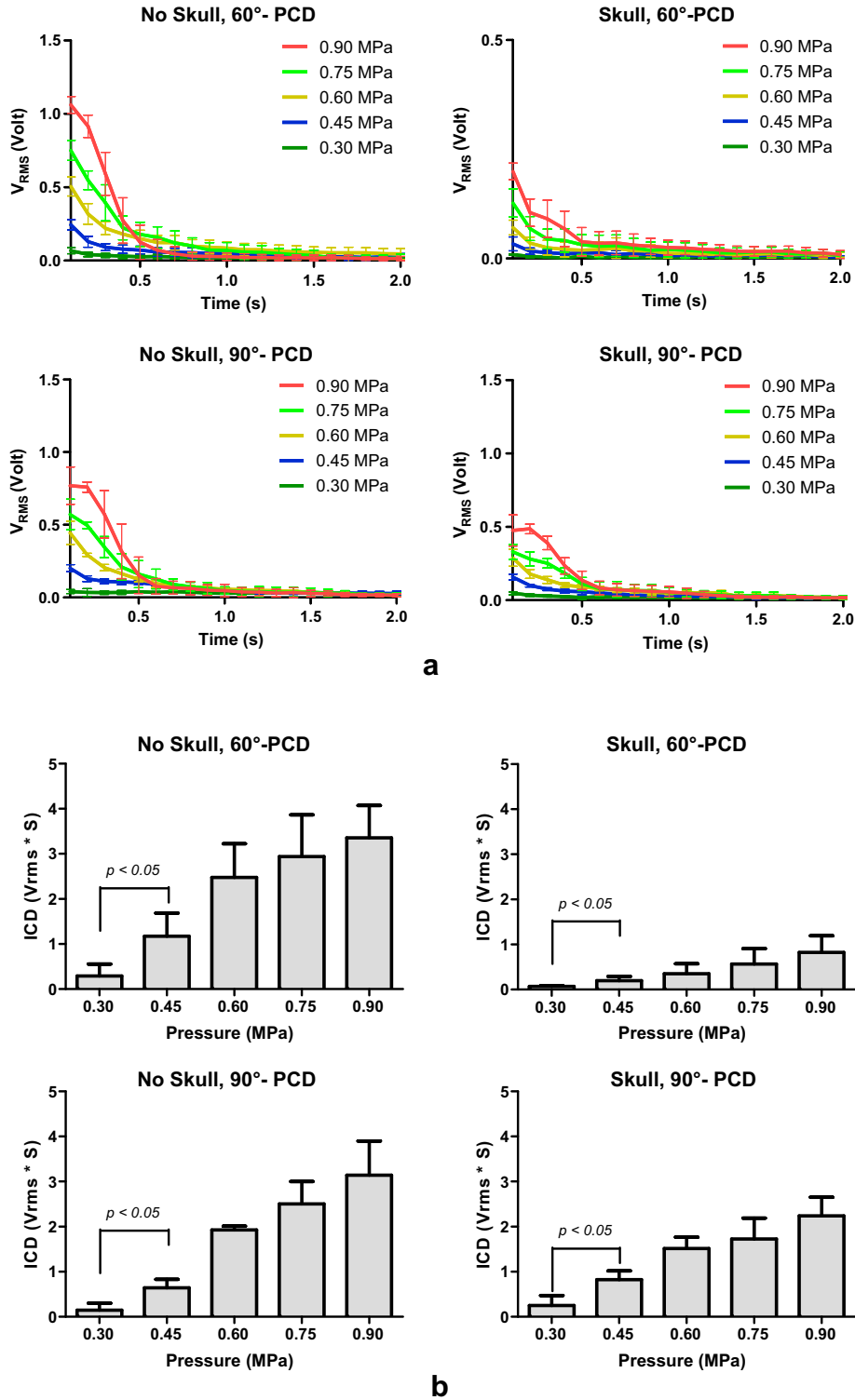


Fig. 5. The (a) root mean square (V_{RMS}) and (b) inertial cavitation dose (ICD) at five distinct acoustic pressures are indicated here. The scale of the 60°-PCD curve (with the skull) was adjusted so that the difference between the curves could be appreciated. The ICD was quantified as the area below the V_{RMS} curve, at each pressure. Twenty pulses were applied for each sonication set. The ICD at 0.45 MPa was significantly larger than at 0.30 MPa ($p < 0.05$) in all cases.

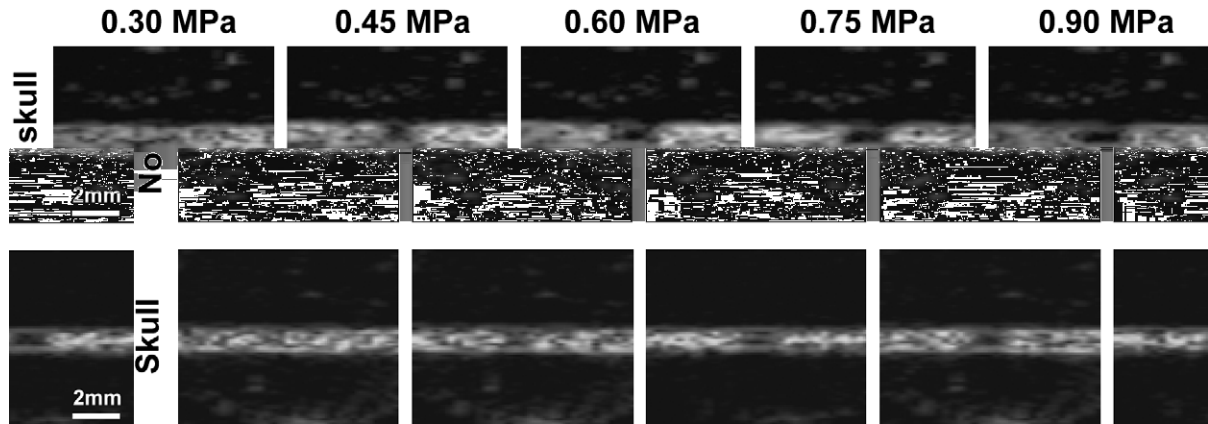


Fig. 6. B-mode imaging provided a means of determining whether the microbubbles were present following sonication. Images were acquired after 2 s of sonication at five distinct acoustic pressures in skull and non-skull experiments.

a skull was investigated in this study. Qualitatively and quantitatively, the threshold of inertial cavitation was identified to be at the peak-rarefactional pressure of 0.45 MPa with or without an *ex vivo* skull in place (Figs. 3 to 7). The frequency spectrum of the first pulse showed that the broadband response appeared when the pressure was at, or higher than, 0.45 MPa (Fig. 3). Spatial mapping using B-mode imaging provided further evidence of bubble disruption caused by inertial cavitation (Fig. 6). The decrease in echogenicity was consistent with the emergence of the broadband response shown in Figure 3, which demonstrated that the microbubbles were disrupted by inertial cavitation. Quantitative results of spatial maps also showed that the image intensity ratio (eqn [1]) at 0.45 MPa was larger than at 0.30 MPa ($p < 0.05$). Hence, both the PCD frequency response and the spatial information from B-mode imaging could be used to determine the threshold of inertial cavitation.

This study also investigated the effect of the skull to predict feasibility in *in vivo* transcranial applications where transcranial cavitation detection is required. At the same pressure amplitude, the ICD was lower in the presence of the skull (Fig. 5b), which showed that the acoustic wave was distorted by the skull. To reduce skull thickness effects being responsible for the difference between the 0° and 60° cases, based on our measurements, the area of the parietal bone, which was assumed to have uniform thickness, was around 5 mm^2 , which would cover the ultrasound path for both the 0° and 60° cases. When the PCD was placed at 60° , the PCD signal amplitude was the lowest because the acoustic wave propagated through the skull twice (Fig. 3b and Fig. 5b). However, the quantification showed that the significant broadband response could still be detected at 60° -PCD (Fig. 5b). Hence, the PCD system used in this study might be suitable for *in vivo* applications.

The broadband response appeared when the microbubbles were sonicated at or above 0.45 MPa. The broadband response at 0.90 MPa persisted for approximately 0.5 s, which was consistent with the V_{RMS} curves (Fig. 5a). Inertial cavitation may have caused microbubble destruction, thus hampering the likelihood of subsequent inertial cavitation. However, harmonics were still detectable during the entire sonication at each pressure amplitude (Fig. 4) and these harmonics appears to have been due to microbubbles (Fig. 8b), as they were absent in the degassed water filled vessel (Fig. 8a). Figure 8 showed that only the 1st and 2nd harmonics appeared when degassed water was sonicated while distinct 1st to 6th harmonics were observed in the presence of microbubbles. There are three possible explanations for this phenomenon. First, since the focal region of the PCD was larger than the focal region of FUS (Fig. 1), the harmonics may be due to the oscillation of microbubbles, which were near the focal region of FUS but had not experienced the full extent of the peak pressure amplitude. Second, some microbubbles may have adhered to the vessel wall and they continued to be acoustically driven. Third, the initial microbubbles may have been disrupted into smaller bubbles, which were not detectable on the B-mode images. These smaller bubbles could then be acoustically driven to emit the characteristic harmonics.

Quantitative results of the frequency response and spatial maps indicated the threshold of inertial cavitation (Fig. 7b). When the pressure was higher than 0.60 MPa, no significant difference was shown in the intensity ratio, since the microbubbles in the focal region might have completely disappeared after 2 s of sonication. In contrast, the ICD increased exponentially when the pressure exceeded the threshold of inertial cavitation.

Here, we provided a simplified method to show that the ICD was influenced by the skull unlike the threshold

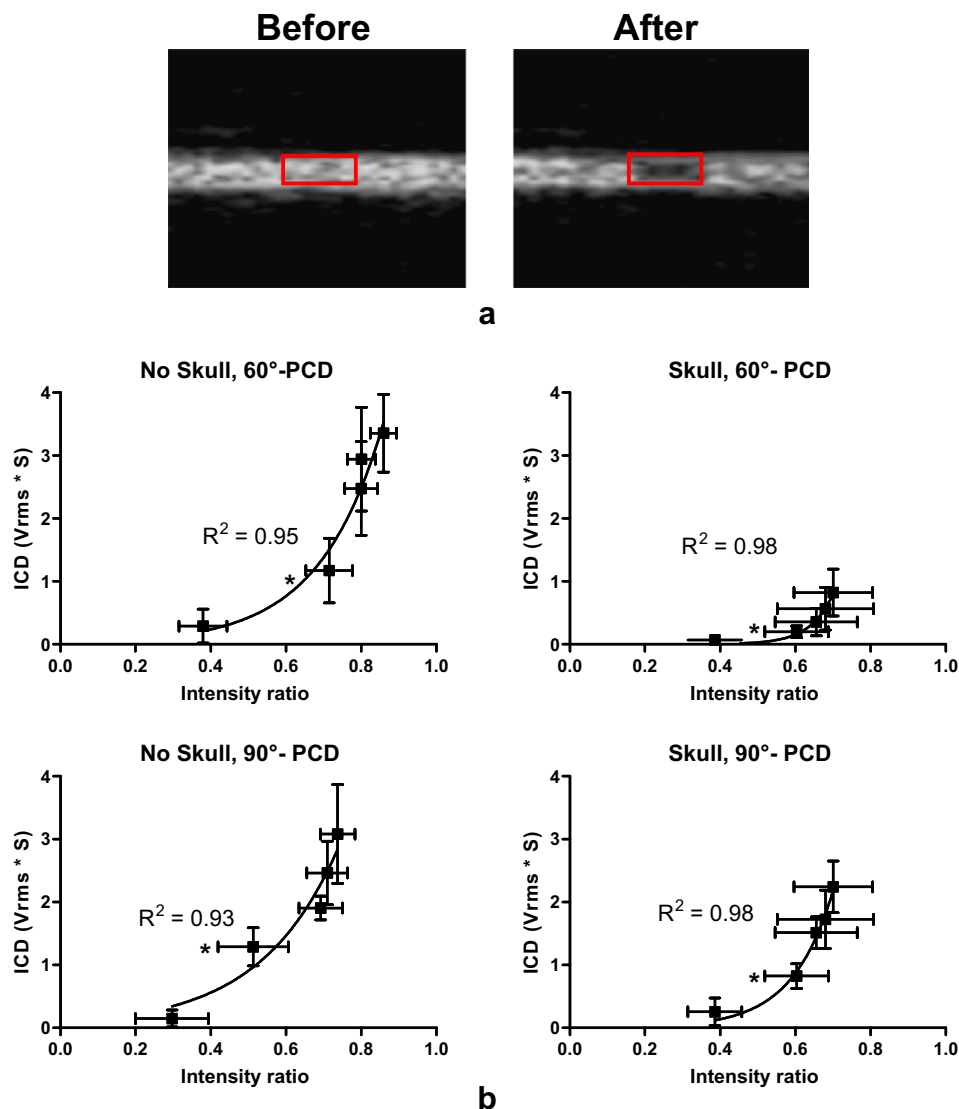


Fig. 7. (a) The illustration of region-of-interest (ROI) and (b) the correlation between inertial cavitation dose (ICD) and the intensity decrease ratio of B-mode imaging at five distinct acoustic pressures (0.30, 0.45, 0.60, 0.75 and 0.90 MPa). The intensity decrease ratio at 0.45 MPa was significantly larger than at 0.30 MPa (*symbol, $p < 0.05$).

of inertial cavitation. This implied that, if the BBB is opened at 0.30 MPa (Choi *et al.* 2010b) the mechanism involved at that pressure may be stable cavitation. However, some issues remain to be investigated further to understand the mechanism of BBB opening. The diameter of the vessel in this study was $610 \mu\text{m}$, which was larger than most murine vessels. The internal carotid artery of the murine brain has a diameter of $218 \pm 19 \mu\text{m}$ (Woitzik *et al.* 2006). The compliance or stiffness of the vessel also influences the bubble behavior (Qin and Ferrara 2006). Therefore, a smaller diameter vessel phantom should be implemented to confirm that the threshold of inertial cavitation of microbubbles within smaller vessels, such as 100 to $300 \mu\text{m}$, will not be affected by the skull.

No flow effects were investigated in the phantom study. The concentration of microbubbles may also affect the threshold of inertial cavitation, which has been shown to decrease with the concentration of microbubbles in the vessel phantom (Sassaroli and Hynynen 2007). The effect of flow and concentration will be investigated in future studies.

The microbubbles used in this study were commercial ultrasound contrast agents. Different contrast agents may have different thresholds of inertial cavitation (Chen *et al.* 2003; Choi *et al.* 2010a). More importantly, most commercial ultrasound contrast agents are poly-dispersed, so the distribution is not symmetrically centered around a certain diameter (Fig. 9). The resonance

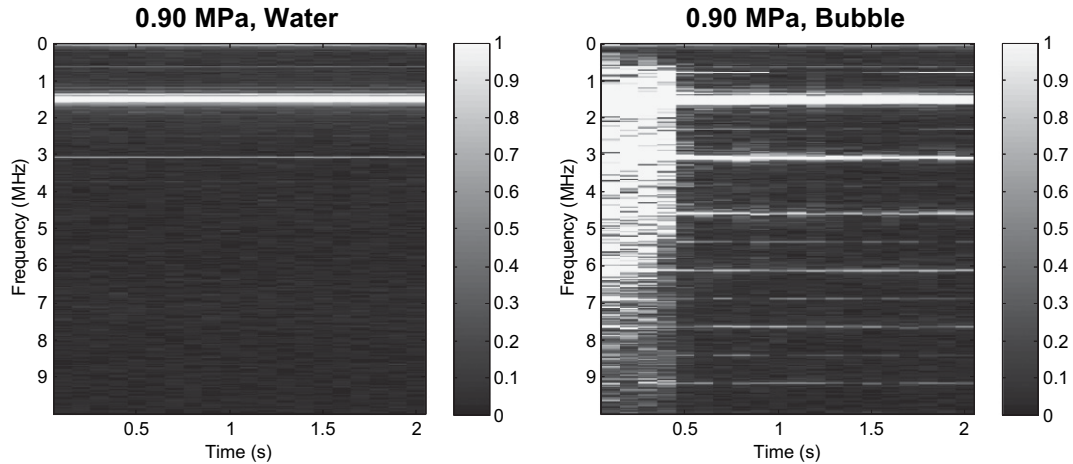


Fig. 8. Comparison between (a) water and (b) bubble experiments without skull for spectrogram from 90° -passive cavitation detector (PCD) at 0.90 MPa. Broadband acoustic emissions and the amplitude of the 3rd to 6th harmonics were not obtained in the water experiments.

frequency of the microbubble varies according to the bubble diameter and shell constituency. Therefore, the size-dependent threshold of inertial cavitation should be investigated to identify the role of different bubble size in inertial cavitation and BBB opening.

The PCD sensitivity also needs to be considered. The broadband response captured by the PCD is dependent on its sensitivity. The results of this study showed that the threshold of inertial cavitation was equal to 0.45 MPa. However, it might be possible that the broadband response was not captured at 0.30 MPa because the PCD sensitivity was not high enough. However, based on the complementary results of the spatial maps from the B-mode imaging, we believe that the sensitivity of the PCD used in this study is sufficiently high.

Two different angles of PCD were used to understand whether the results will be influenced by the presence of the skull. At 0.30 MPa without the skull, some signal at 60° -PCD (Fig. 3a) was higher than at 90° -PCD (Fig. 3c). The signals obtained by 60° -PCD may include some reflected signals from the surface of the phantom, which may not have been captured by 90° -PCD. The PCD used in this study had a cylindrical focus, which was ideal when the hydrophone was positioned perpendicular to the focused ultrasound transducer's main axis. When positioned in this manner, the cylindrical focal region closely matches the cigar shape of the FUS focal spot (Fig. 1b). If the PCD is placed at 60° relative to the focused ultrasound transducer's main axis, other reflected signals from the surface of the phantom and the effect of the skull will also be observed. Therefore, it may be better to place the PCD at 90° for vessel phantom experiments and demonstrate the feasibility of transcranial PCD measurements for in vivo applications in which PCD can only be placed above the skull.

Preliminary results of *in vivo* transcranial cavitation detection during BBB opening using the same set-up are shown in Figure 10. The spectrogram during the first 0.2 ms of sonication demonstrated that the broadband acoustic emissions were detected at and beyond the peak-rarefactional pressure of 0.45 MPa and no broadband acoustic emissions were detected at 0.30 MPa, which

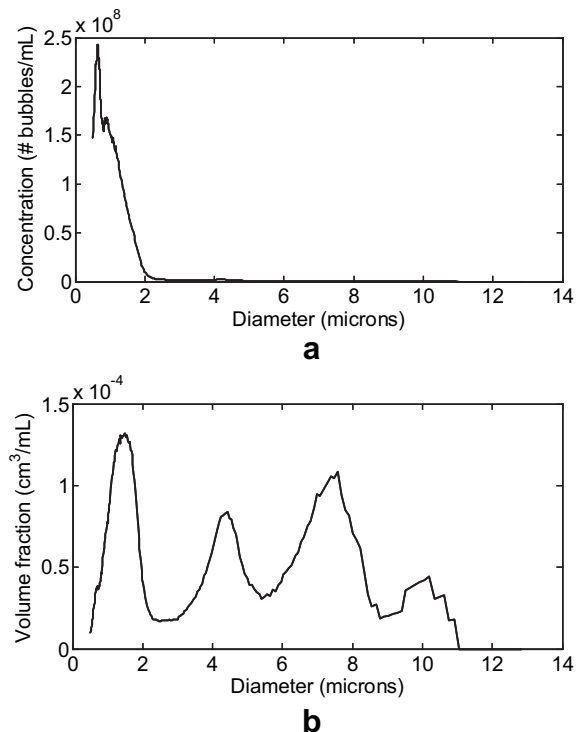


Fig. 9. The size distribution of the Definity microbubbles (a) according to the number concentration and (b) volume fraction was characterized. This indicated that the Definity microbubbles were polydispersed.

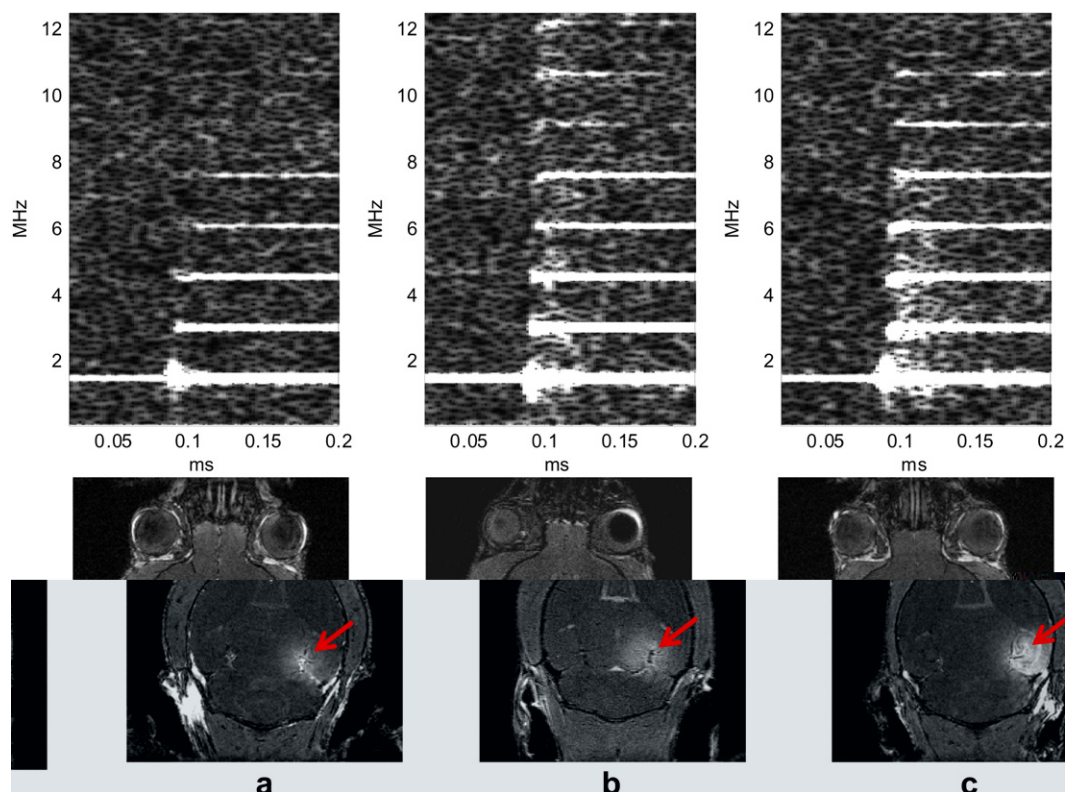


Fig. 10. Spectrogram during the first 0.2 ms sonication. Broadband acoustic emissions were detected at (b) 0.45 MPa and (c) 0.60 MPa but not at (a) 0.30 MPa. Corresponding MRI images confirm that the blood-brain barrier (BBB) could be opened at 0.30 MPa, *i.e.*, without inertial cavitation. The red arrows indicate the location of BBB opening.

were consistent with our phantom study findings. Our results on the IC threshold are independent on the number of cycles and thus potential standing wave effects. The vessel size and blood flow might be additional factors affecting the acoustic response. The effects of vessel size, blood flow and bubble concentrations will be studied in future studies. Post-sonication MRI showed that the BBB could be opened at 0.3 MPa without the evidence of any broadband acoustic emissions. Therefore, the BBB might be opened without requiring inertial cavitation.

CONCLUSION

In this article, we investigated the threshold of inertial cavitation transcranially using FUS and microbubbles in a vessel phantom. We demonstrated that: (1) the threshold of inertial cavitation is not influenced by the mouse skull; (2) if the pressure remains the same, the presence of the skull will result into a lower inertial cavitation dose but will not influence the inertial cavitation threshold. The signal of inertial cavitation could be detected transcranially and *in vivo* with the PCD device currently used. In the future, *in vivo* transcranial BBB

opening with cavitation detection will be investigated to unveil the mechanism of BBB opening.

Acknowledgements—This study was supported in part by NIH R21EY018505, NIH R01EB009041 and NSF CAREER 0644713. The authors appreciate Keith Yeager, Department of Biomedical Engineering, Columbia University, for making the hydrophone holder used in this study. The authors also appreciate Shunichi Homma, M.D., Department of Cardiology, Columbia University, for providing microbubbles (Definity) used in this study. The authors also thank Thomas Deffieux, Ph.D., Jonathan Vaupou, Ph.D., Jianwen Luo, Ph.D., and Wei-Ning Lee, Ph.D., Jean Provost, M.S., Department of Biomedical Engineering, Columbia University, for their helpful discussions.

REFERENCES

- Ammi AY, Cleveland RO, Mamou J, Wang GI, Bridal SL, O'Brien WD Jr. Ultrasonic contrast agent shell rupture detected by inertial cavitation and rebound signals. *IEEE Trans Ultrason Ferroelectr Freq Control* 2006;53:126–136.
- Apfel RE, Holland CK. Gauging the likelihood of cavitation from short-pulse, low-duty cycle diagnostic ultrasound. *Ultrasound Med Biol* 1991;17:179–185.
- Chen WS, Brayman AA, Matula TJ, Crum LA. Inertial cavitation dose and hemolysis produced *in vitro* with or without Optison. *Ultrasound Med Biol* 2003a;29:725–737.
- Chen WS, Brayman AA, Matula TJ, Crum LA, Miller MW. The pulse length-dependence of inertial cavitation dose and hemolysis. *Ultrasound Med Biol* 2003b;29:739–748.
- Chen WS, Matula TJ, Brayman AA, Crum LA. A comparison of the fragmentation thresholds and inertial cavitation doses of different ultrasound contrast agents. *J Acoust Soc Am* 2003;113:643–651.

- Choi JJ, Pernot M, Brown TR, Small SA, Konofagou EE. Spatio-temporal analysis of molecular delivery through the blood-brain barrier using focused ultrasound. *Phys Med Biol* 2007a;52:5509–5530.
- Choi JJ, Pernot M, Small SA, Konofagou EE. Noninvasive, transcranial and localized opening of the blood-brain barrier using focused ultrasound in mice. *Ultrasound Med Biol* 2007b;33:95–104.
- Choi JJ, Feshitan JA, Baseri B, Wang S, Tung YS, Borden MA, Konofagou EE. Microbubble-size dependence of focused ultrasound-induced blood-brain barrier opening in mice *in vivo*. *IEEE Trans Biomed Eng* 2010a;57:145–154.
- Choi JJ, Wang S, Tung YS, Morrison B 3rd, Konofagou EE. Molecules of various pharmacologically-relevant sizes can cross the ultrasound-induced blood-brain barrier opening *in vivo*. *Ultrasound Med Biol* 2010b;36:58–67.
- Chomas JE, Dayton P, Allen J, Morgan K, Ferrara KW. Mechanisms of contrast agent destruction. *IEEE Trans Ultrason Ferroelectr Freq Control* 2001a;48:232–248.
- Chomas JE, Dayton P, May D, Ferrara K. Threshold of fragmentation for ultrasonic contrast agents. *J Biomed Opt* 2001b;6:141–150.
- Farny CH, Holt RG, Roy RA. Temporal and spatial detection of HIFU-induced inertial and hot-vapor cavitation with a diagnostic ultrasound system. *Ultrasound Med Biol* 2009;35:603–615.
- Giesecke T, Hynynen K. Ultrasound-mediated cavitation thresholds of liquid perfluorocarbon droplets *in vitro*. *Ultrasound Med Biol* 2003;29:1359–1365.
- Hynynen K, McDannold N, Sheikov NA, Jolesz FA, Vykhodtseva N. Local and reversible blood-brain barrier disruption by noninvasive focused ultrasound at frequencies suitable for trans-skull sonications. *Neuroimage* 2005;24:12–20.
- Hynynen K, McDannold N, Vykhodtseva N, Jolesz FA. Noninvasive MR imaging-guided focal opening of the blood-brain barrier in rabbits. *Radiology* 2001;220:640–646.
- Hynynen K, McDannold N, Vykhodtseva N, Raymond S, Weissleder R, Jolesz FA, Sheikov N. Focal disruption of the blood-brain barrier due to 260-kHz ultrasound bursts: A method for molecular imaging and targeted drug delivery. *J Neurosurg* 2006;105:445–454.
- Leighton TG. *The Acoustic Bubble*, 1994.
- McDannold N, Vykhodtseva N, Hynynen K. Targeted disruption of the blood-brain barrier with focused ultrasound: Association with cavitation activity. *Phys Med Biol* 2006;51:793–807.
- McDannold N, Vykhodtseva N, Hynynen K. Use of ultrasound pulses combined with Definity for targeted blood-brain barrier disruption: A feasibility study. *Ultrasound Med Biol* 2007;33:584–590.
- McDannold N, Vykhodtseva N, Hynynen K. Blood-brain barrier disruption induced by focused ultrasound and circulating preformed microbubbles appears to be characterized by the mechanical index. *Ultrasound Med Biol* 2008a;34:834–840.
- McDannold N, Vykhodtseva N, Hynynen K. Effects of acoustic parameters and ultrasound contrast agent dose on focused-ultrasound induced blood-brain barrier disruption. *Ultrasound Med Biol* 2008b;34:930–937.
- McDannold N, Vykhodtseva N, Raymond S, Jolesz FA, Hynynen K. MRI-guided targeted blood-brain barrier disruption with focused ultrasound: Histological findings in rabbits. *Ultrasound Med Biol* 2005;31:1527–1537.
- Miller MW, Miller DL, Brayman AA. A review of *in vitro* bioeffects of inertial ultrasonic cavitation from a mechanistic perspective. *Ultrasound Med Biol* 1996;22:1131–1154.
- Qin S, Ferrara KW. Acoustic response of compliant microvessels containing ultrasound contrast agents. *Phys Med Biol* 2006;51:5065–5088.
- Sassaroli E, Hynynen K. On the impact of vessel size on the threshold of bubble collapse. *Appl Phys Lett* 2006;89:123901.
- Sassaroli E, Hynynen K. Cavitation threshold of microbubbles in gel tunnels by focused ultrasound. *Ultrasound Med Biol* 2007;33:1651–1660.
- Takegami K, Kaneko Y, Watanabe T, Maruyama T, Matsumoto Y, Nagawa H. Polyacrylamide gel containing egg white as new model for irradiation experiments using focused ultrasound. *Ultrasound Med Biol* 2004;30:1419–1422.
- Talu E, Powell RL, Longo ML, Dayton PA. Needle size and injection rate impact microbubble contrast agent population. *Ultrasound Med Biol* 2008;34:1182–1185.
- van Wamel A, Bouakaz A, Versluis M, de Jong N. Micromanipulation of endothelial cells: Ultrasound-microbubble-cell interaction. *Ultrasound Med Biol* 2004;30:1255–1258.
- Woitzik J, Hecht N, Schneider UC, Pena-Tapia PG, Vajkoczy P. Increased vessel diameter of leptomeningeal anastomoses after hypoxic preconditioning. *Brain Res* 2006;1115:209–212.